Experimental study of runup for sandy beaches under waves and tide

Alaa Khoury, Armelle Jarno, François Marin

▶ **To cite this version:**

Alaa Khoury, Armelle Jarno, François Marin. Experimental study of runup for sandy beaches under waves and tide. Coastal Engineering, 2019, 144, pp.33-46. 10.1016/j.coastaleng.2018.12.003 . hal-02116268

HAL Id: hal-02116268
https://hal.science/hal-02116268

Submitted on 4 Apr 2022

HAL is a multi-disciplinary open access archive for the deposit and dissemination of scientific research documents, whether they are published or not. The documents may come from teaching and research institutions in France or abroad, or from public or private research centers.

L'archive ouverte pluridisciplinaire **HAL**, est destinée au dépôt et à la diffusion de documents scientifiques de niveau recherche, publiés ou non, émanant des établissements d'enseignement et de recherche français ou étrangers, des laboratoires publics ou privés.

Experimental study of runup for sandy beaches under waves and tide

Alaa Khoury
alaa.khoury@univ-lehavre.fr

Armelle Jarno*
jarnoa@univ-lehavre.fr

François Marin
francois.marin@univ-lehavre.fr

Laboratoire Ondes et Milieux Complexes, UMR CNRS 6294, Université Le Havre Normandie, 25 rue Philippe Lebon, B.P. 1123, 76063, Le Havre cedex, France

*Corresponding author.

Abstract

This paper describes an experimental investigation of runup for intermediate sandy beaches from a physical modelling in a wave flume with tide simulation. Shoreline elevation measurements are acquired over a wide range of conditions using an optical method. Simultaneous morphological and hydrodynamic changes are considered to determine the best parameters to predict the maximum wave runup. The tidal level significantly affects the breaking conditions (position, height and type), and the slopes of the beach. Present data show that the surf zone slope and the wave breaking height should be used to estimate the maximum runup. The results are compared with previous formulations issued from the literature. A new formula is proposed for the runup estimation for intermediate beaches.

Keywords: Intermediate beach type; Waves; Tide; Runup; Swash; Physical modelling

1 Introduction

The swash zone is an important zone to study for two main reasons. It is a place of intense sediment transport (Masselink and Hughes, 1998; Puleo et al., 2000) and constitutes the interface between the shore and the sea. It has therefore been the subject of numerous studies (Hunt, 1959; Battjes, 1974; Guza and Thornton, 1982; Holman, 1986; Mase, 1989; Nielsen and Hanslow, 1991; van der Meer and Stam, 1992; Komar, 1998; Ruggiero et al., 2001; Hedges and Mase, 2004; Stockdon et al., 2006; Cariolet, 2011; Cariolet and Suanez, 2013; Blenkinsopp et al., 2016; Park and Cox, 2016). An important engineering work for coastal protection is to predict accurately wave runup. Extreme wave runup is expressed in terms of the vertical elevation exceeded by the largest 2% of waves ($R_{2\%}$) (Hunt, 1959; Battjes, 1974; Holman, 1986; Mase, 1989; Nielsen and Hanslow, 1991; van der Meer and Stam, 1992; Komar, 1998; Ruggiero et al., 2001; Hedges and Mase, 2004; Stockdon et al., 2006; Blenkinsopp et al., 2016; Park and Cox, 2016) or by its maximum value ($R_{\max}$) (Mase, 1989; Komar, 1998; Cariolet, 2011; Cariolet and Suanez, 2013). Studies dedicated to runup parameterization can be differentiated according to different criteria. First, studies are performed whether in laboratory from small-scale (van der Meer and Stam, 1992) to prototype-scale (Blenkinsopp et al., 2016) installations or in field conditions (Guza and Thornton, 1982; Holman, 1986; Nielsen and Hanslow, 1991; Komar, 1998; Ruggiero et al., 2001; Stockdon et al., 2006; Cariolet, 2011; Cariolet and Suanez, 2013). Then, waves can be regular or irregular. The domain of monochromatic waves is restricted to laboratory simulations while irregular wave conditions can be performed in some laboratory facilities and define obviously the standard case of field investigations. Another criterion refers to the tidal regime that can vary from microtidal - for a great majority of studies - to macrotidal. Megatidal conditions characterized by a tidal range superior to 8 m (Levoy et al., 2000) are rarely studied. Beaches are classified reflective, intermediate or dissipative according to Wright and Short classification (Wright and Short, 1984) based on the values of the dimensionless fall velocity (Dean number) (Dean, 1973): $\Omega = H_b/W_sT$, where H_b is the breaking wave height, W_s the sediment fall velocity and T the wave period. They can be plane, concave or exhibiting complex topographies, with bars or berms, or extended with more than one slope for long intertidal zones. Furthermore, beaches can be impermeable for laboratory studies or porous for natural beaches and for a few laboratory studies (van der Meer and Stam, 1992; Blenkinsopp et al., 2016).

All of these specificities do not lead to an abundance of predictors. Three main type-equations were proposed in the literature focusing on intermediate and reflective beaches. More complex forms were proposed by Ruggiero et al. (2001) and Stockdon et al. (2006). However, very few studies deal with the case of intermediate beaches (Holman, 1986; Komar, 1998; Stockdon et al., 2006; Cariolet, 2011; Cariolet and Suanez, 2013). Each type-equation was validated by laboratory and field studies. These equations are given in Table 1 with a non-exhaustive list of studies. Constants and exponents in the equations are fitted to environmental or laboratory conditions and the choice of the

slope differs according to authors. For many of them, the foreshore slope (β_f) is the most adapted to predict runup on natural beaches (Nielsen and Hanslow, 1991; Ruggiero et al., 2001; Stockdon et al., 2006; Sabatier et al., 2009). It is also easy to measure even under storm conditions. However, some authors have considered that the surf zone slope (βs) influences the runup distribution for complex topographies and can be more representative of the beach face (Holman, 1986; Nielsen and Hanslow, 1991; Komar, 1998; Stockdon et al., 2006). Only a few authors used β_s for runup parameterization (Holman, 1986; Komar, 1998). For macrotidal beaches, Cariolet et al. (Cariolet, 2011) proposed to use the active beach slope (βa) defined as the mobile upper part of the beach. The authors argued that in macrotidal environments, the use of the average foreshore slope can also be problematic because the intertidal zone is extended and generally not homogeneous.

Table 1 Principal formulae proposed in the literature to estimate the wave runup. Hydro- and morphodynamic conditions are given for each study.

alt-text: Table 1

Type	Equation	Study (L: Laboratory; F: Field)		R	Constants	Eq.	Slope	Beach type	Tidal regime
1	$\frac{R}{H_0} = C\xi$	Hunt (Hunt, 1959)	L	$R_{2\%}$	$C = 1$	(5)	β	Smooth and rough plane slopes	–
		Battjes (Battjes, 1974)	L	$R_{2\%}$	C= (1.49–1.87)	(6)	β	Smooth and impermeable	–
		Nielsen and Hanslow (Nielsen and Hanslow, 1991)	F	$R_{2\%}$	$C = 1.188$	(7)	β_f	Reflective ($\beta \geq 0.10$)	Micro-
		van der Meer and Stam (van der Meer and Stam, 1992)	L	$R_{2\%}$	$C = 0.96$	(8)	β	Smooth and rock slopes ($\xi < 1.5$)	–
		Komar (Komar, 1998)	F	$R_{2\%}$ R_{max}	$C = 0.92$ $C = 1.07$	(9)	β_s	Intermediate	–
						(10)			
		Stockdon et al. (Stockdon et al., 2006)	F	$R_{2\%}$	$C = 0.73$	(11)	β_f	Reflective ($\xi > 1.25$)	Micro- to meso-
		Cariolet (Cariolet, 2011)	F	R_{max}	$C = 1.09$	(12)	β_a	Intermediate	Macro-
		Cariolet and Suanez (Cariolet and Suanez, 2013)	F	R_{max}	$C = 0.67$	(13)	$\beta_a = \beta_f$	Intermediate	Macro-
2	$\frac{R}{H_0} = C_1\xi + C_2$	Holman (Holman, 1986)	F	$R_{2\%}$	$C_1 = 0.83$; $C_2 = 0.2$	(14)	β_s	Intermediate to reflective	Micro-
		Hedges and Mase (Hedges and Mase, 2004)	L	$R_{2\%}$	$C_1 = 1.49$; $C_2 = 0.34$	(15)	β	Smooth and impermeable slopes	–
		Blenkinsopp et al. (Blenkinsopp et al., 2016)	L	$R_{2\%}$	$C_1 = 0.795$; $C_2 = 0.39$	(16)	β_f	Reflective	–
3	$\frac{R}{H_0} = C\xi^{\alpha}$	Mase (Mase, 1989)	L	$R_{2\%}$ R_{max}	$C = 1.86$; $\alpha = 0.71$ $C = 2.32$; $\alpha = 0.77$	(17)	β	Gentle and impermeable slopes	–
						(18)			
		van der Meer and Stam (van der Meer and Stam, 1992)	L	$R_{2\%}$	$C = 1.17$; $\alpha = 0.46$	(19)	β	Smooth and rock slopes ($\xi > 1.5$)	–
		Blenkinsopp et al. (Blenkinsopp et al., 2016)	L	$R_{2\%}$	$C = 1.165$; $\alpha = 0.77$	(20)	β_f	Reflective	–
		Park and Cox (Park and Cox, 2016)	L	$R_{2\%}$	$C = 1.35$; $\alpha = 0.65$	(21)	β_f	–	–
4	$\frac{R}{H_0} = C\xi^{\alpha}\left(\frac{H_0}{L_0}\right)^k$	Ruggiero et al. (Ruggiero et al., 2001)	F	$R_{2\%}$	$C = 0.27$; $\alpha = 0.5$; $k = 0.25$	(22)	β_f	Reflective	Meso-
5	$\frac{R}{H_0} = 0.385\,\xi + 0.413\left[\xi^2 + \frac{7.1\times10^{-3}}{H_0/L_0}\right]^{0.5}$	Stockdon et al. (Stockdon et al., 2006)	F	$R_{2\%}$	–	(23)	β_f	All types of beaches	Micro- to meso-
6	$\frac{R}{H_0} = C\sqrt{\frac{L_0}{H_0}}$	Nielsen and Hanslow (Nielsen and Hanslow, 1991)	F	$R_{2\%}$	$C = 0.099$	(24)	-	Dissipative ($\beta < 0.10$)	Micro-

		Stockdon et al. (Stockdon et al., 2006)	F	$R_{2\%}$	$C = 0.043$	(25)	–	Dissipative ($\xi < 0.3$)	Micro- to meso-
7	$\frac{R}{H_0} = C_1 + \frac{C_2}{H_0}$	Guza and Thornton (Guza and Thornton, 1982)	F	R_s	$C_1 = 0.71$; $C_2 = 0.035$ m	(26)	–	Dissipative	–
		Ruggiero et al. (Ruggiero et al., 2001)	F	$R_{2\%}$	$C_1 = 0.5$; $C_2 = -0.22$ m	(27)	–	Dissipative	Meso-

In most of predicting equations, the maximum runup is normalized by the deep water significant wave height (H_0). Whereas this data is easy to acquire in laboratory as mentioned by Stockdon et al. (2006) and Blenkinsopp et al. (2016), the field valid deep water wave height data must be estimated properly in order to correlate correctly the runup with the waves driving it.

Type-Equation (1):

The basis form of the normalized runup height, historically the first one and the most extensively used:

$$\frac{R}{H_0} = C\xi \quad \textbf{(1)}$$

was established from laboratory studies by Hunt (1959) and reformulated by Battjes (1974) through Iribarren number ξ (Iribarren and Nogales, 1949):

$$\xi = \beta / \sqrt{H_0 / L_0} \quad \textbf{(2)}$$

where β is the beach slope, L_0 is the deep water wavelength and C is a dimensionless constant. It predicts a linear dependence of R/H_0 with the Iribarren number. Beach slope was plane, uniform and impermeable. This formula which was used more recently in another laboratory study (van der Meer and Stam, 1992), was further supported by natural environments on particular beaches (Komar, 1998; Cariolet, 2011; Cariolet and Suanez, 2013) or by extensive datasets on a variety of beaches and conditions (Nielsen and Hanslow, 1991; Stockdon et al., 2006). Substantial higher runup values are found for plane impermeable small scale laboratory beaches than for natural beaches. Even if laboratory beaches are rough or composed of two slopes, a more partial transfer of energy to the shore is found for natural beaches where the beach slope is less uniform, and where granulometry may vary along the beach and processes of infiltration/exfiltration can act effectively.

Type-Equation (2):

$$\frac{R}{H_0} = C_1\xi + C_2 \quad \textbf{(3)}$$

is an adjusted parameterization to take account for a setup level, where C_1 and C_2 are constant values. Thus, when the beach becomes flat, runup tends to a non-zero value. Some laboratory investigations (Hedges and Mase, 2004; Blenkinsopp et al., 2016) and field studies (Holman, 1986) validate this form of equation. Blenkinsopp et al. (2016) found a setup contribution varying approximately between 14% for the steeper beaches tested ($\xi = 3$) to 33% for the milder beaches ($\xi = 1$). The swash runup always constitutes the more significant portion of total runup.

Type-Equation (3):

$$\frac{R}{H_0} = C\xi^{\alpha} \quad \textbf{(4)}$$

was introduced by Mase and Iwagaki (1984) and Mase (1989) for laboratory studies with random waves on gentle smooth and impermeable slopes. Recently, the same equation form was used to describe permeable small-scale beach in laboratory (van der Meer and Stam, 1992), a prototype-scale reflective barrier beach (Blenkinsopp et al., 2016) and in a numerical model based on Boussinesq equation (Park and Cox, 2016). This equation is little used in-situ.

For dissipative and ultra-dissipative beaches studied in the field, other parameterizations were proposed (Type-Equations 6 and 7; Table 1). The dependence on beach slope becomes negligible (Hanslow and Nielsen, 1993) and incident water wave height plays a major role in runup estimation. Runup at infragravity frequencies grows with increasing values of $(H_0 L_0)^{1/2}$ while at incident frequencies it saturates (Guza and Thornton, 1982; Holman and Sallenger, 1985; Ruessink et al., 1998; Stockdon et al., 2006; Senechal et al., 2011).

Some studies deal with runup without proposing parameterization (Guedes et al., 2011). Thus, in the field experiments of Holman and Sallenger (1985) and Guedes et al. (2011), the tide influence was pointed out for microtidal intermediate beaches. Significant runup height varied by a factor of 2 between low tide and high tide, demonstrating in the case of a barred beach the influence of the water level (Guedes et al., 2011). Furthermore, according to these

authors, the energy at infragravity frequencies increases at low tide by a mechanism of energy transfer from the incident band where this infragravity modulation seems to be connected with the presence of secondary waves.

The variation of water level constitutes a source of variability of runup by variation of beach slope and by modification of breaking conditions. This paper investigates these two influences from small-scale laboratory tests performed on an intermediate sandy beach exposed to controlled waves and tide.

2 Experimental setup and measurement techniques

2.1 Experimental setup

The experiments have been performed in a small-scale wave flume with 10.7 m length, 0.49 m width and 0.5 m high at LOMC laboratory (UMR CNRS 6294), University of Le Havre (France). Based on Froude similitude for waves and tides generation, the length and temporal scales were fixed to 1/100 and 1/10 respectively. The scaling for the sediment transport and the beach profile is based on the dimensionless sediment fall velocity (Dean number (Dean, 1973)). Saleh Salem et al. (Saleh Salem et al., 2011) and Khoury et al. (2013) studied the capacity to reproduce the main features of sand beach morphologies in this small-scale installation. They have shown that for Dean number in the same range as for natural beaches ($2.3<\Omega<4.9$), equilibrium intermediate beaches according to Wright and Short classification (Wright and Short, 1984) are well reproduced in this flume. They have also succeeded in generating both erosive and accretive wave conditions. A comparison between results obtained in the present flume and results obtained in bigger flumes for a same value of the Dean number ($\Omega = 3.6$) was conducted by Saleh Salem (Saleh Salem, 2011) to study the scale effect. In this way, the large-scale Hannover wave flume GWK (307 m) and the medium scale Barcelona wave flume CIEM (100 m) were considered (Sánchez-Arcilla et al., 2011). The scale ratio for Barcelona and present flumes with respect to the Hannover flume are 1:1.9 and 1:20, respectively. The comparison of beach profiles obtained in the present installation with those obtained in the GWK and CIEM flumes shows that the main characteristics are fairly well reproduced in the present small-scale flume.

The experimental setup is schematized in Fig. 1. The oscillating-type wave generator is located at one side of the flume and a sandy beach exposed to both waves and tides is located at the other end.

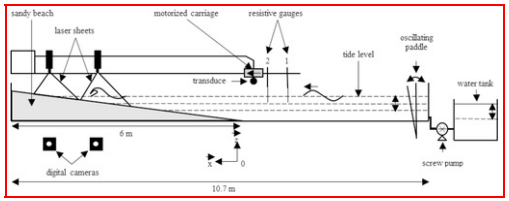

Fig. 1 Side view of the flume.

alt-text: Fig. 1

The mean water level was varied to simulate a 12 h tidal period (72 min at the flume scale) with a 10 m tidal range (100 mm at the flume scale) using a screw pump. Tidal cycle was modelled by generating a succession of four phases: low tide (duration: 1h40min), rising tide (duration: 4h20min), high tide (duration: 1h40min) and falling tide (duration: 4h20min). The tide variation fixed to 100 mm in the channel induces a low value of the relative tidal range ($RTR<3$).

2.2 Measurement techniques

The incident wave characteristics were measured using two resistive gauges (Fig. 1). The wave reflection estimated following Goda et al. (Goda, 2000) varied between 5% and 10%. To enable direct comparison with previous studies, the deepwater wave height and wave length were then calculated by de-shoaling the waves out to deep water using linear wave theory.

A 12 composite-element array of ultrasonic sensors developed by Seatek company mounted on a motorized carriage was used for 3D-mapping of the beach. In order to measure both sub-aerial and submerged beach elevations, the flume was slowly filled with water before each bathymetric acquisition. The vertical accuracy is estimated to be 0.5 mm. The horizontal distance between two profiles, fixed by the carriage speed, is 1.3 mm.

The free surface and bed level were video recorded in the breaker and swash zones. A vertical light sheet directed along the longitudinal axis of the flume induces a light line on the free surface and on the bed in the studied zones; this line was video recorded using a HD video camera (JVC GZ-HD) (1920×1080) located aside the channel (Fig. 1). A typical camera calibration procedure is used with a grid standard that has a predetermined grid spacing with an accuracy greater than 1/10th of a millimeter. The calibration is performed by recording an image of this grid in order to determine the correspondence between the camera and the real world. This process was repeated multiple times, once for each new measurement. The spatial resolution is 0.5 mm/pixel and the length of the observation field is 1 m. The observation window was moved during tests to follow zones of interest during the tidal cycle. In spite of the repetitive task that it implies, a manual processing routine was adopted to track with accuracy successive elevations of the shoreline, bed slope and breaking parameters (breaking height, position and water depth) from videos.

The image analysis gave qualitative information on the characteristics of the free surface near the breaking zone. The horizontal coordinate corresponding to the vertical tangent of the free surface was considered as the wave breaking point (Fig. 2). The breaking wave height, H_b, and the water depth, h_b, were precisely measured at this point using the Matlab software. An automatic detection in these interfacial regions has been tested and rapidly abandoned because of a weak capacity to capture accurately the edge of a thin moving water layer at the shore or a mobile breaking zone.

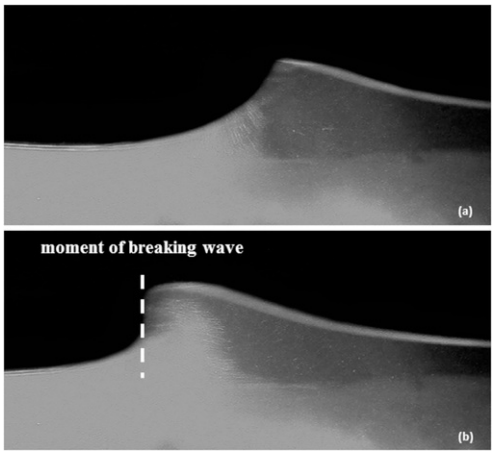

Fig. 2 Wave profile (a) before and (b) at the breaking point. At the moment of wave breaking, the tangent is vertical (vertical dashed line).

alt-text: Fig. 2

The water level time-series at the shore were also extracted from videos. The successive horizontal and vertical positions were manually acquired using Matlab. One swash event tracked at 25 Hz was processed every 30 s for the rising, falling and high tide phases. Fig. 3 illustrates a sequence of images which show clearly the highest point of the water-air interface. The instant and the tidal level for which this maximum was reached were precisely measured with the resistive probe 1 (Fig. 1).

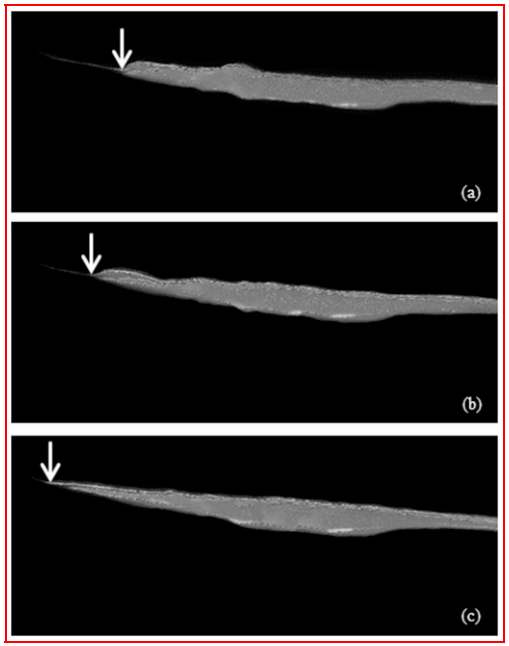

Fig. 3 Example of instantaneous shoreline detection during the rising phase of water level.

alt-text: Fig. 3

2.3 Tests initial conditions

Regular waves were generated. The 6 m initial length beach profiles were entirely made of well-sorted natural sand ($\sigma_g^2<2$) (Soulsby, 1997), where σ_g is the geometric standard deviation $\sigma_g = \sqrt{D_{84}/D_{16}}$ and D_{16} and D_{84} diameters are the grain size for which 16% and 84% of the sample, respectively, is finer. Tests were carried out with very fine ($D_{50} = 111$ µm, where D_{50} is the median sediment diameter) or fine sand ($D_{50} = 173$ µm) of relative density s = 2.65.

Six different test conditions were performed (Table 2). The duration of each test was sufficiently long to reach equilibrium profile. A bottom evolution velocity was used to determine when the profile reaches equilibrium (Grasso et al., 2009a; Saleh Salem et al., 2011). We consider that the equilibrium state is reached when the mean beach profile velocity tends towards a fixed low value (<2 mm/h).

Table 2 Initial test conditions.

alt-text: Table 2

Nº test	Excitation type	Hydrodynamic parameters				Control parameters		Initial state of the beach
		h (mm)	T (s)	H (mm)	H_0 (mm)	Ω	RTR	(P: Plane; B: Barred)
1	waves	280	1.0	38	42	4.9	0	P with 2 slopes
2	waves and tide	180–280	1.0	27–41	29–45	4.9	2.3	B
3	waves	230	1.0	38	42	2.3	0	P with 2 slopes
4	waves and tide	180–280	1.0	27–41	29–45	2.3	2.3	B
5	waves and tide	180–280	1.0	35–58	38–64	2.6	2.0	P with 3 slopes
6	waves and tide	200–300	1.0	33–55	36–60	2.6	2.0	B

For Test 1, the initial plane profile composed of two slopes (1:9 for the lower part (1000 mm) and 1:17 for the upper part of the beach) was exposed to waves for 144 h ($T = 1$ s; $H_0 = 38$ mm; $h = 280$ mm). The test conditions lead to an intermediate beach profile with a Dean number of 4.9. The equilibrium profile is characterized by a steep slope in the upper part of the beach ($\beta = 0.358$), a dissipative section located in the lower part ($\beta = 0.028$) and a well-marked subtidal bar (Fig. 4a). The equilibrium profile for Test 1 was then exposed to 8 tidal cycles (9h36 min at the flume scale) ($RTR = 2.3$) with the same waves conditions (Test 2). The tide leads to the formation of an intertidal bar at the equilibrium state (Fig. 4a). For Test 2, the upper part of the beach is protected at the equilibrium state by the presence of the intertidal bar and the amplitude of swash oscillations is negligible.

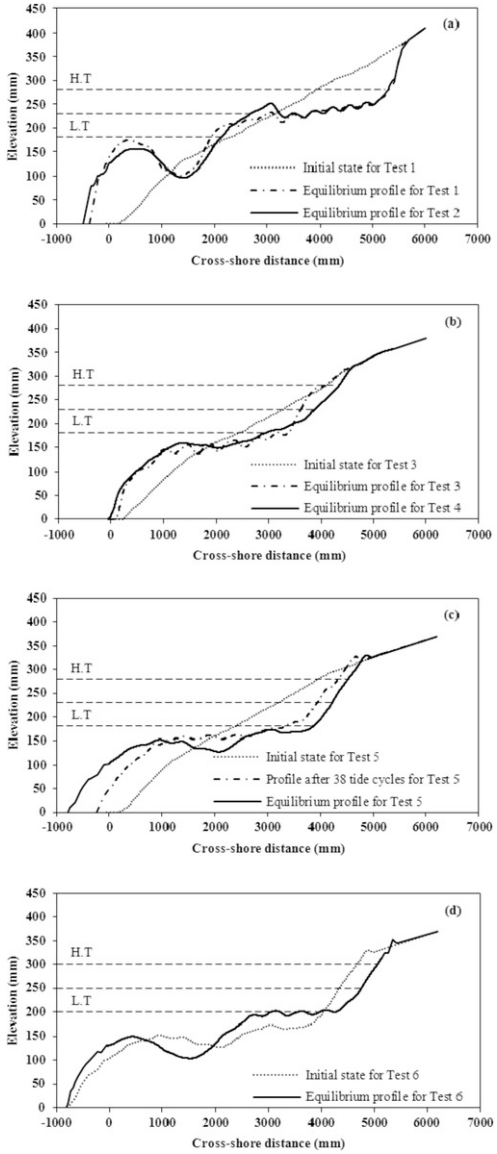

Fig. 4 Beach profiles (a) at the equilibrium state for Tests 1 and 2, (b) at the equilibrium state for Tests 3 and 4, (c) after 38 tide cycles for Test 5 (Test 5.a) and at the equilibrium state for Tests 5 (Test 5.b), and (d) at the equilibrium state for Test 6. The dashed lines refer to the still water level at low (L.T), mean and high (H.T) tides.

alt-text: Fig. 4

For Test 3, an initial plane beach composed of two slopes (1:9 for the lower part (1000 mm) and 1:17 for the upper part of the beach) was exposed to waves for 95 h ($T = 1$ s; $H_0 = 38$ mm; $h = 230$ mm) till an equilibrium profile typical of the intermediate-reflective domain ($\Omega = 2.3$) was reached with a steep beach face ($\beta = 0.178$) (Fig. 4b). The equilibrium profile of Test 3 was then submitted to 12 tidal cycles (14h24 min at the flume scale) ($RTR = 2.3$) with the same waves conditions (Test 4). The equilibrium beach profile shaped by both waves and tide is used to study the runup for a whole tidal cycle. It was characterized by a non-marked subtidal bar, a weaker slope in the lower part of the beach ($\beta = 0.038$) and a steeper slope in the upper part ($\beta = 0.115$) (Fig. 4b).

For Test 5, the initial plane beach composed of three slopes (1:9 for the lower part of the beach (1000 mm), 1:17 for the intermediate part (3000 mm) and 1:25 for the upper part) was exposed to both waves ($T = 1$ s; $H_0 = 45$ mm; $h = 230$ mm) and tide ($RTR = 2.0$) from the beginning of the test for 38 cycles (45h36 min at the flume scale). The value of the Dean number was $\Omega = 2.6$. For this test, the equilibrium state was not reached. The high tide phase was first investigated (Test 5.a).

Test 5 was then completed until equilibrium state was obtained after 76 tide cycles (91h12 min at the flume scale). The tide induces a strong erosion of the upper part of the beach with an increase of its slope (Fig. 4c). The equilibrium beach profile was used to study the runup at high tide phase (Test 5.b). It is characterized by a pronounced subtidal bar and a steep upper beach slope ($\beta = 0.159$) (Fig. 4c). Once the equilibrium state was reached for Test 5, the water level was increased ($h = 250$ mm) with the same tidal range and same waves conditions (Test 6). Runup at high tide was studied at the equilibrium state after 27 tidal cycles (32h24 min at the flume scale) (Fig. 4d).

3 Results

3.1 Hydrodynamic conditions

3.1.1 Breaking conditions

3.1.1.1 Breaking positions ***(New line after the subtitle 3.1.1.1 please. Be careful, next lines are not correctly justified at right.)***

Successive breaking points were spotted from videos, and horizontal distances (X_s) from the breaker point where onset of wave breaking were observed to the instantaneous shoreline were calculated and plotted during the tidal cycle on Fig. 5a as a function of time for Test 4. This distance represents the width of the surf zone (Stockdon et al., 2006) where energy partly dissipates before waves reach the shore.

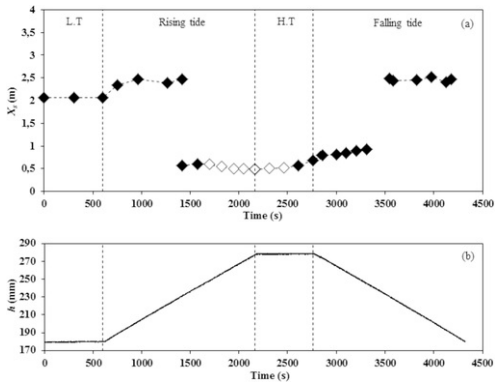

Fig. 5 (a) Positions of breaking point during the tidal cycle for Test 4. $t = 0$ refers to the beginning of low tide phase; X_s refers to the distance from the shoreline. Solid diamonds: spilling breaking; open diamonds: plunging breaking at the shore. (b) Tide water level.

alt-text: Fig. 5

The complex beach profile associated to a variation of the water level is responsible for a complex evolution of breaking conditions. Wave breaking occurs at a distance between 2 m and 2.5 m from the instantaneous shoreline for water depths ranging from the low tide level ($h = 180$ mm) to the mean water level ($h = 230$ mm), corresponding to instants in the simulated tide cycle between $t = 600$ s and $t = 1380$ s (Fig. 5a). The surf zone is extended for these water levels. Breaking occurs above the slightly marked subtidal bar present in the lower part of the profile. When the depth is around mean water level ($h = 230$ m, $t = 1421$ s), two breaking points are detected; the first one further offshore is due to the subtidal bar whose effect vanishes with the water level increase and the second one to the arrival to the shore.

When the water level exceeds $h = 230$ mm, the bar does not induce anymore breaking and only persists the point of breaking close to the shore. Its location around $X_s = 500$ mm in the second part of the rising phase moves slightly offshore at the end of high tide ($X_s = 700$ mm for $h = 280$ mm at $t = 2645$ s). The point of breaking continues to move slightly offshore in the first part of the falling phase. It reaches $X_s = 900$ mm for $h = 230$ mm at $t = 3305$ s (Fig. 5a). This progressive movement of the breaking point is significant. It results from changes in the slope of the breaking zone in relation to local slope changes of the beach profile. For higher water levels than the mean water level, the breaking point is closer to the shore during rising phase than falling phase. For example, for $h = 248$ mm, $X_S = 600$ m in rising phase ($t = 3305$ s) while $X_s = 900$ mm in falling phase ($t = 1700$ s). On the other hand, for lower levels than $h = 230$ mm, the positions are almost equal for the two phases (around $X_s = 2500$ mm). This stability of breaking point is explained by the similarity of the lower part of the beach during the two phases as a consequence of a weak sediment transport in this zone.

For Tests 5.a, 5.b and 6, the position of breaking point is relatively stable at high tide ($X_s = 800$ mm for Test 5.a, $X_s = 400$ mm for Test 5.b and $X_s = 600$ mm for Test 6).

3.1.1.2 Height and type of breaking waves *(New line after the subtitle 3.1.1.2 please. The next lines are not correctly justified at right.)*

The breaking type is characterized by the Iribarren number ξ based on the breaking wave height and the local slope at the breaking point. The wave breaking height was experimentally measured at low, mean and high tide levels using the optical method described in Section 2.2. The measurements for present test were compared to the following formulae proposed by Goda (1970) (Eq. (28)), Komar and Gaughan (1972) (Eq. (29)) and Nielsen (2009) (Eq. (30)), in order to choose the most appropriate formula for our study:

$$H_b = 0.17\, L_0 \left\{ 1 - \exp\left[-1.5\, \frac{\pi\, h_b}{L_0} \left(1 + 15\, \beta_b^{4/3} \right) \right] \right\} \quad \textbf{(28}$$

$$H_b = 0.56\, H_0^{4/5} L_0^{1/5} \quad \textbf{(29}$$

$$H_b = \left[\frac{\gamma_b}{4\, k_0}\, H_0^4\, cos^2 \alpha_0 \right]^{1/5} \quad \textbf{(30}$$

where γ_b is the breaker index, $K_0 = 2\pi/h_b$ and α_0 represents the incident wave angle ($\alpha_0 = 0$ in our case).

Estimated values of the breaking wave height are compared with the measured values on Fig. 6. These data were acquired during the tests and not only at the equilibrium state. The values of γ_b and β_b vary over a wide range, from 0.31 to 0.93 for γ_b and from 0.020 to 0.196 for β_b. This shows the complexity of breaking conditions for the intermediate studied beaches for which the bathymetry is complex. It appears that when breaking is localized near the shore, H_b obtained by the Goda formula (Goda, 1970) underestimates the wave breaking heights (Fig. 6). In the other hand, the Goda formula (Goda, 1970) tends to overestimate these heights when the breaking occurs far from the shore (Fig. 6). Whatever the breaking conditions, the formula of Nielsen (2009) tends to underestimate wave breaking heights (Fig. 6). Finally, we can observe that our results are in good agreement with those predicted using the Komar and Gaughan formula (Komar and Gaughan, 1972) with a root-mean-square error (*RMSE*) of 2.17 mm (Fig. 6). The results obtained and discussed in Section 3.1.1.1 show that, on barred profiles the breaking point position changes significantly during the tidal cycle. It shifts from the sandbar at low tide toward the shoreline at high tide. For this reason, the breaking wave height for other water levels, when it's not easy to measure breaking conditions, was alternatively calculated using the Komar and Gaughan formula (Komar and Gaughan, 1972).

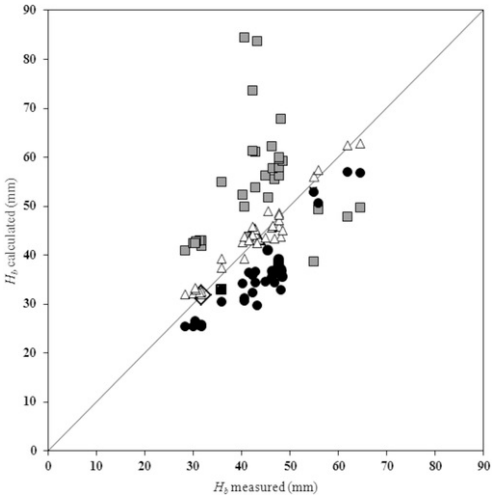

Fig. 6 Comparison between measured and calculated H_b values for Tests 1, 2, 4 and 6 – square symbols: Goda (1970); triangle symbols: Komar and Gaughan (1973); circle symbols: Nielsen (2009).

alt-text: Fig. 6

Nielsen criterion (Nielsen, 2009) was applied to predict the breaking type and validated by direct observation of the breaking zone: if $\xi_b < 0.4$, spilling breaking is observed, when plunging breaking occurs for $0.4 < \xi_b < 2$. Changes of breaking type are mainly controlled by slope changes in the breaking zone. Two changes occur during the tide cycle for Test 4 (Table 3). The first one coincides with the onshore shifting of the breaker zone when the water level increases. Breaking is spilling characterized by ξ_b values between 0.19 and 0.36 for tide levels between 180 mm and 250 mm. It becomes plunging for higher levels when it takes place at a short distance from the shore where slopes are steeper. The Iribarren number increases from 0.19 to 0.88. The second change - from plunging to spilling - occurs at the end of high tide when the upper beach flattens inducing a slight offshore displacement of the breaking point in a zone where the slope is milder ($\beta_b = 0.04$). For Test 5.a, Test 5.b and Test 6, Iribarren numbers at high tide are equal respectively to 1.09, 1.13 and 0.87. No change of breaking type is observed for these tests; the breaking type remains plunging.

Table 3 Breaking type during the tide cycle at the equilibrium state for Test 4.

alt-text: Table 3

	L.T	Rising phase			H.T		Falling phase	
h (mm)	180	180–236	237–250	251–280	280	280	280–237	236–180
β_b	0.06	0.06	0.04	0.17	0.17	0.04	0.04	0.06
ξ_b	0.36	0.36	0.19	0.88	0.85	0.21	0.22	0.36
Breaking type	spilling	spilling	spilling	plunging	plunging	spilling	spilling	spilling

3.2 Morphodynamic conditions

In this section, the different slopes that are considered when runup is questioned are estimated.

The active section of the beach – section characterized by the greatest altitudinal variability - was introduced by Cariolet (2011). We choose to determine this zone from beach profiles measured by the acoustic technique at the end of low and high tides (Fig. 7). The beach profile is less steep and smoother at low tide than at high tide, as shown for Tests 4, 5.a, 5.b and 6 on Fig. 7. The net change in altitude Δh calculated between these two profiles gives the two limits of the active section of the upper beach. It represents between one-half and two-thirds of the upper part of the intertidal zone (Fig. 7). The active slopes for Tests 4, 5.a, 5.b and 6 are respectively 0.115, 0.124, 0.146 and 0.122.

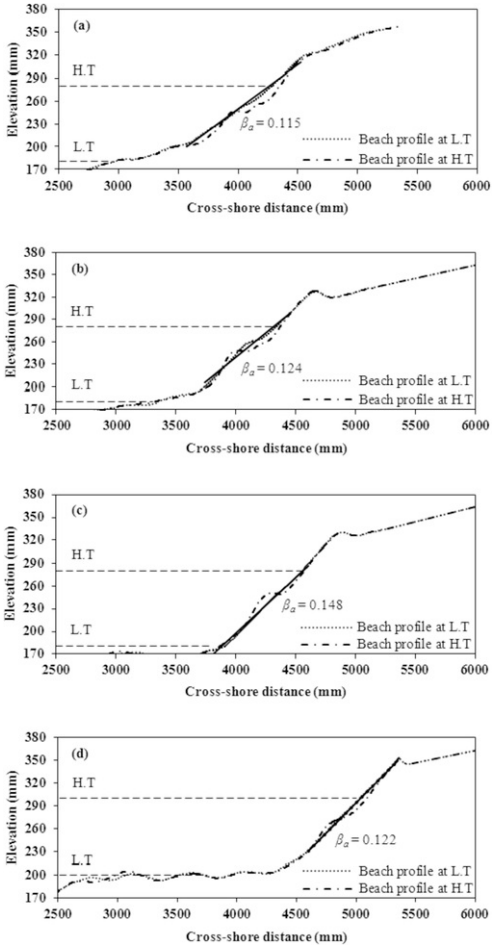

Fig. 7 Beach profiles at the end of low and high tides for (a) Test 4, (b) Test 5.a, (c) Test 5.b and (d) Test 6. The solid line refers to the active slope of the beach (β_a). The dashed lines refer to the still water level at low (L.T) and high (H.T) tides.

alt-text: Fig. 7

3.2.1 Foreshore slope (β_f)

During the tidal cycle, a dynamic beach profile was defined by the movement of the swash zone to different parts of the beach face. It was processed from the optical monitoring of the swash zone for Test 4. The foreshore beach slope was then estimated according to Stockdon et al. (2006) as the slope in the region defined by $\pm 2\sigma$ of the shoreline position time series around the mean shoreline position $<\eta>$.

The studied beach exhibits marked changes in bed gradient while the tidal level evolves during the rising and falling tide phases, changes which are estimated by the use of slope segments with high values of the regression coefficient ($0.94 < R^2 < 0.99$). The dynamic profile measured during the rising tide is more complex than in the falling tide (Fig. 8). Five segments are necessary to follow accurately the evolution of the swash zone during the rising tide (Fig. 8a) whereas four are enough for the falling phase (Fig. 8b). The foreshore slope varies in a relatively wide range, between 0.049 and 0.194. Differences between bed slopes are located in the upper part of the beach. During the rising phase, the upper beach is defined by two slopes while only a single slope is enough for the falling tide. The smoothing of beach profile observed during the falling phase explains this regularity (Section 3.2.1). The lower part of the beach extending from low tide to mean water level is divided in two similar segments for the two phases. The upper and lower parts of the beach are separated by an intermediate zone with a gentle slope. This zone is more extended during the rising tide than the falling tide (Fig. 8).

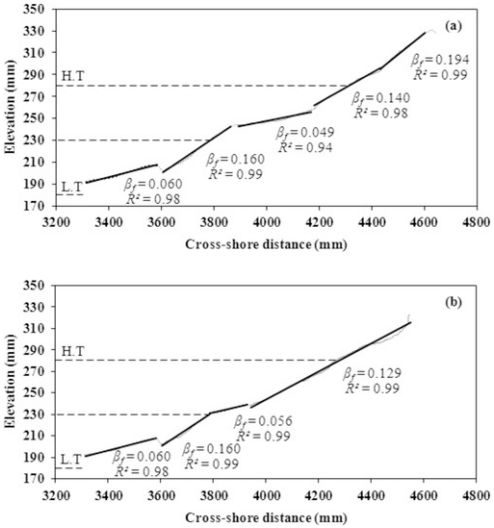

Fig. 8 Dynamic beach profiles measured by optical method during (a) rising tide and (b) falling tide at the equilibrium state for Test 4. The solid line refers to the foreshore beach slope (β_f). The dashed lines refer to the still water level at low (L.T), mean and high (H.T) tides.

alt-text: Fig. 8

During high tide phase, the same part of the beach was solicited for a long time with the same hydrodynamic forcing and morphological changes were observed. The foreshore slope was measured at the beginning (B.H.T), middle (M.H.T) and end (E.H.T) of high tide for Tests 4, 5.a, 5.b and 6 (Fig. 9). Results are summarized in Table 4.

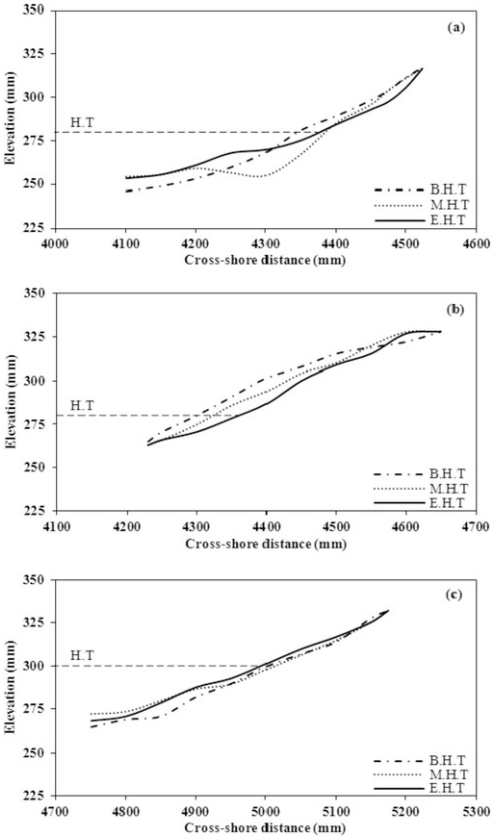

Fig. 9 Morphological evolution of the upper part of the beach during high tide for the beginning (B.H.T), middle (M.H.T) and end (E.H.T) of the phase for (a) Test 4, (b) Test 5.a and (c) Test 6. The dashed line refers to the still water level at high tide (H.T).

alt-text: Fig. 9

Table 4 Average foreshore slope during high tide for the beginning (B.H.T), middle (M.H.T) and end (E.H.T) of the phase for Tests 4, 5.a, 5.b and 6.

alt-text: Table 4

Nº test	B.H.T	M.H.T	E.H.T
4	0.193	0.193	0.131
5.a	0.144	0.175	0.191
5.b	0.180	0.180	0.180
6	0.182	0.182	0.182

The most significant morphological changes take place at the end of high tide phase for Test 4 (Fig. 9a). They are directly related to the erosion of the upper part of the beach leading to a decrease in the foreshore slope from 0.193 to 0.131 (Table 4). This type of morphological changes was also observed in-situ on a macrotidal Breton beach (France) (Cariolet, 2011). For the non-equilibrium test (Test 5.a), a continuous erosion in the swash zone is observed causing the increase of the foreshore slope (Fig. 9b and Table 4). On the other hand in the case of the equilibrium beach profile of Test 5.b and Test 6 (Fig. 9c), the beach profile is slightly translated with no significant change detected on the foreshore slope (Table 4).

3.2.2 Surf zone slope (β_s)

The average surf zone slope was calculated according to Stockdon et al. (2006) as the slope between the shoreline and the cross-shore location of wave breaking. The average slope was measured in the surf zone corresponding to each of the foreshore slopes estimated in Section 3.2.2 as shown in Table 5. The surf zone slope was not estimated when two breaking points were detected (Table 5).

Table 5 Average foreshore and surf zone slopes estimated during the tidal cycle for Test 4 and during the high tide phase for Tests 5.a, 5.b and 6.

alt-text: Table 5

Nº test	phase	h (mm)	β_f	β_s
4	Rising	190–208	0.060	0.022
		209–243	0.160	0.022
		244–257	0.049	–
		258–294	0.140	0.078
		295–330	0.194	0.099
	High tide	280	0.193	0.083
			0.131	0.095
	Falling	330–239	0.129	0.109
		238–230	0.056	–
		229–208	0.160	0.022
		207–190	0.060	0.022
5.a	High tide	280	0.144	0.121
			0.175	0.121
			0.191	0.121
5.b	High tide	280	0.180	0.111
6	High tide	300	0.182	0.126

For Test 4, the surf zone slope varies between 0.022 and 0.109. The steepest slope has been observed at the beginning of the falling tide whereas the weakest has been measured for low water levels during the rising and falling phases. The stability of the slope for these levels is due to the low reactivity of the beach profile and to wave breaking over the subtidal bar which leads to a wide surf zone. For $h > 230$ mm, the surf slope changes more rapidly, due to wave breaking at the shoreline.

For Tests 5.a, 5.b and 6, the surf zone slopes are respectively 0.121, 0.111 and 0.126. They do not vary during high tide phase. The slope of the surf zone does not seem correlated with the foreshore slope ($R^2 = 0.34$) as shown in Fig. 10.

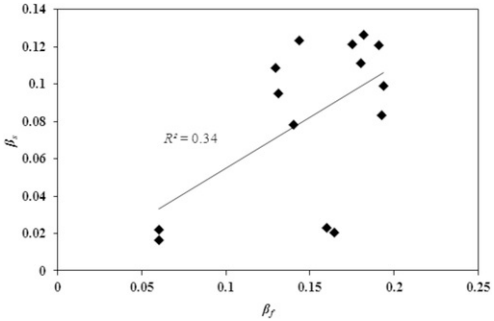

Fig. 10 Surf zone slope plotted as a function of the foreshore slope for Tests 4, 5.a, 5.b and 6.

alt-text: Fig. 10

3.3 Hydrodynamics of swash zone over a tide cycle

In this section, we first globally describe the evolution of the time series and then in the discussion section, the signal is decomposed into three parts: the wave runup *R(t)* corresponding to the maximum water level reached (uprush level), the swash height *S(t)* measured between rundown and uprush level of the selected swash event, and the setup $<\eta>(t)$ corresponding to the time-averaged water-level elevation at the shoreline for a more detailed analysis.

3.3.1 Rising and falling tide phases

Fig. 11 presents the shoreline elevation time-series for the rising and falling phases, for $h > 190$ mm water levels. Lower water levels were not processed due to the small amplitudes of swash events which were difficult to detect and anyway not affecting the beach. In order to compare the rising and falling tide, the two phases are divided into three time-periods characterized by a different localization of the breaking zone according to our preceding observations (Fig. 11). For A-zone ($190\,\text{mm} < h < 225\,\text{mm}$), breaking occurs far from the shore, triggered by the subtidal bar. B-zone ($225\,\text{mm} < h < 235\,\text{mm}$) refers to a transition zone where two successive breaking points were detected and C-zone, corresponding to higher water levels ($h > 235$ mm), is characterized by a bathymetric breaking near the shore.

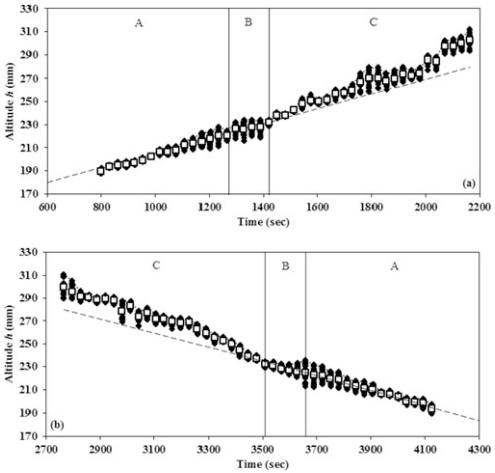

Fig. 11 Shoreline elevation time-series for (a) rising tide and (b) falling tide for Test 4. Origin ($t = 0$) refers to the beginning of low tide. Dashed line: deep water level; solid diamonds: successive elevations of the water level at the shore; open squares: mean water level at the shore. A B and C refer to zones identified by different breaking conditions. A - breaking on subtidal bar, B - two breaking points and C - breaking at the shore.

alt-text: Fig. 11

3.3.2 High tide phase

The signal undergoes important modifications during the 10 min of high tide (Fig. 12). For half of the high tide duration, rundown limit moves towards slightly lower values that the high tide level. During the last one hundred seconds, the swash zone is shortened due to the rise of the rundown level. This evolution is the consequence of the morphological and hydrodynamic changes observed.

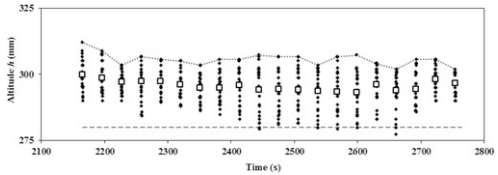

Fig. 12 Shoreline elevation time-series at high tide for Test 4. Origin (t = 0) refers to the beginning of low tide. Dashed line: deep water level; solid diamonds: successive elevations of the water level at the shore; open square: mean water level at the shore.

alt-text: Fig. 12

4 Discussion

4.1 Evolution of wave runup, swash height and wave setup during the tidal cycle

4.1.1 Rising and falling tide phases

R(t), S(t) and $<\eta>(t)$ are normalized by the deep wave height (H_0) at the considered water level. Fig. 13 compares the evolution of R/H_0, S/H_0 and $<\eta>(t)$ as a function of the tidal level for the rising and falling tide. Breaking zones are also shown on this figure.

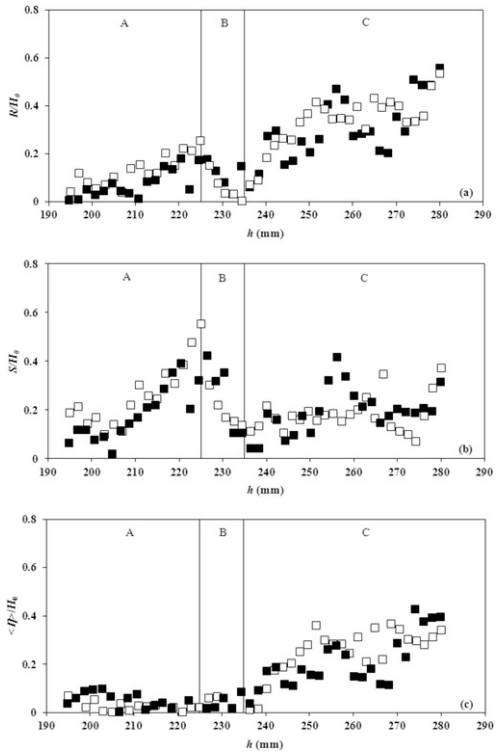

Fig. 13 Variation of (a) relative wave runup, (b) swash height and (c) wave setup with water level for rising and falling tide for Test 4. Solid squares: rising phase; open squares: falling phase. A, B and C refer to zones identified by different breaking conditions. A - breaking above the subtidal bar, B - two breaking points and C - breaking at the shore.

alt-text: Fig. 13

A-zone: data for rising and falling tides show similar evolutions. Both R/H_0 and S/H_0 increase/decrease linearly with the tidal level in rising/falling tide (Fig. 13). For this zone, the incident wave and breaking point are the same for the two phases at constant water level. In addition, the beach profile in its lower part is similar ($\beta_s = 0.022$) when h increases or decreases. Consequently, it is normal that the water level at the shore varies identically for the two phases. The values of $<\eta>/H_0$ are very low when waves dissipate over the bar. It demonstrates that the setup component is controlled exclusively by H_0 in a region where the surf zone slope is mild ($\beta_s = 0.022$). This result is consistent with the field study of Holman and Sallenger (1985) where a loss of dependence of setup with Iribarren number was found for the lowest tides.

B-zone: two breaking points were detected in this zone. Fig. 13 shows a change of dependency of R/H_0 and S/H_0 with the tidal level for the two phases: R/H_0 and S/H_0 decrease linearly as the tidal level increases. The decrease of runup and swash heights, in spite of a steep foreshore slope ($\beta_f = 0.160$), is due to the two successive wave breakings that limit the wave energy reaching the shoreline. The setup component remains low in this zone, characterized by a mild slope in the surf zone ($\beta s = 0.022$).

C-zone: unlike the A-zone, differences between both phases are observed. Fig. 13 clearly shows that the two components vary slightly more irregularly with h during the rising tide and do not follow the same trend when the water level rises or falls. Fig. 13a highlights the dependence of R/H_0 with the tidal level. Runup measured when waves break near the shoreline (C-zone) is more than twice as great as the one measured when wave breaking occurs over the subtidal bar far from shore (A-zone). The results of our physical modelling concerning tidal control are consistent with field measurements by Holman and Sallenger (1985) and Guedes et al. (2011) for barred intermediate microtidal beaches. Furthermore, as observed on the water level time-series (Fig. 11), R/H_0 evolves much more regularly with time in the falling phase than in the rising phase. This is particularly evident for $h > 235$ mm where the breaking point is located near the shoreline (zone C). The smoothing process of beach profile in the falling phase explains this regularity. Indeed, we have shown that the beach profile is more complex in rising tide than during the falling tide (Section 3.2.2). The swash height is relatively constant for this zone, with the exception of a peak around h = 256 mm in rising phase. The wave setup increases linearly as the tidal level increases. It reaches approximately 22 mm at the end of rising tide, which is 39% of the offshore wave height ($H_0 = 57$ mm). This result is consistent with the field study performed by Nielsen (1988) for Dee Why Beach (Sydney, Australia), which mentioned that the shoreline setup is about 40% of the offshore wave heights H_{0rms}, that is about 45% of the offshore mean wave heights H_0m, assuming a Rayleigh probability distribution function. On the other hand, present values are higher than expected by Guza and Thornton (1981) for Torrey Pines Beach (San Diego, California), which does not show any well-developed bar structure ($\beta = 0.02$). According to these authors, the setup at the shoreline corresponds approximately to 17% of the significant wave height in deep water, that is about 27% of the mean wave height in deep water. It is important to mention that the present values of setup are imposed by the surf zone slope varying between 0.099 in rising phase and 0.109 in falling phase (Table 5). A similar loss of dependence was also reported by Stockdon et al. (2006) in field studies on barred intermediate and reflective beaches. They showed that the setup parameterization was improved using an Iribarren-like form ($\xi_0 H_0$) for the higher tidal levels. Furthermore, Guza and Thornton (1981) noted that their results could be different on barred beaches.

4.1.2 High tide phase

Part of the processed swash events is depicted in Fig. 14. The temporal evolution of swash events is more irregular at the beginning and middle than at the end of high tide. A clear similarity between successive swash events is only found at the end of the phase (Fig. 14c). Although the beach is in equilibrium state for the studied tidal cycle, it evolves during this long phase of high tide at constant water level during which energetic waves reach the shore. Breaking position moves slightly offshore during the high tide phase and the foreshore slope decreases due to erosion of the upper part of the beach. The regularity and similarity of successive swash events observed at the end of the phase tends to confirm that the beach has finally reached a quasi-equilibrium state for this water level. (Figure 14 is at the right place in the proof file but must be rotated to be horizontal (90 degree anticlockwise))

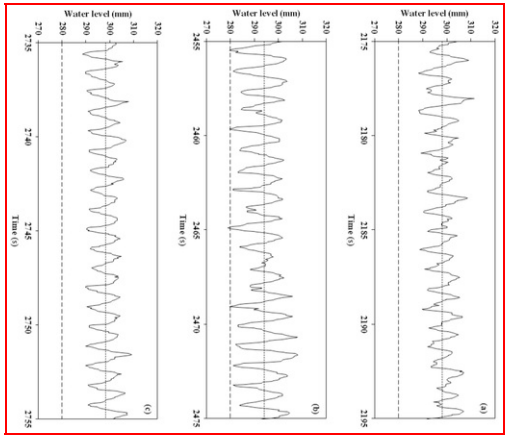

Fig. 14 Water-level time-series at the shore during high tide for the (a) beginning, (b) middle and (c) end of the phase. The dashed line refers to the still water level at high tide. The dotted line refers to the wave setup.

alt-text: Fig. 14

The energy calculated on 40 successive swash events at the beginning, middle and end of high tide shows that wash energy is concentrated in the incident frequency band as expected for intermediate - reflective beaches (Senechal et al., 2011). It evolves from 0.14 J/m3 at the beginning to 0.45 J/m3 in the middle and 0.20 J/m3 at the end of high tide. The wave setup at high tide phase varies between 13 and 20 mm (Fig. 12). The maximum value corresponds to 35% of the offshore wave height ($H_0 = 57$ mm), which is consistent with Nielsen (1988) results.

4.2 Runup parametric study

In this section, hydrodynamic and morphodynamic parameters are investigated: incident wave height, breaking position, breaking type, foreshore slope and surf slope. Let us call R_{max} the maximum runup measured among individual runup events.

Fig. 15 displays the variation of R_{max} with the deep wave height (H_0). A clear linear dependence between the runup and the incident wave height is observed during the tidal cycle ($R^2 = 0.93$) without noticeable influence of the change of breaking location by tidal modulation on this relationship.

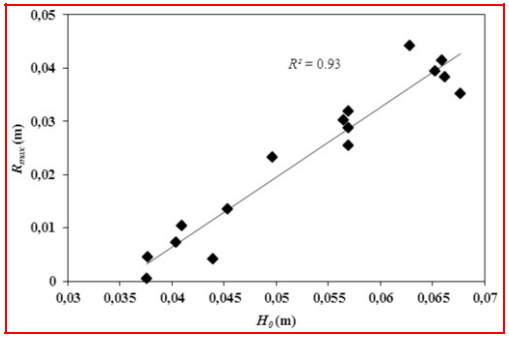

Fig. 15 Variation of the maximum runup with the deep wave height.

alt-text: Fig. 15

The dependence of normalized runup R_{max}/H_0 with the foreshore slope is analyzed through the Iribarren number ξ_f based on the deep wave height and the foreshore slope (Fig. 16). It is shown that the linear runup dependence on the foreshore slope reported in previous studies (Nielsen and Hanslow, 1991; Stockdon et al., 2006; Blenkinsopp et al., 2016) does not seem to be as clear in this study where the tide level changes ($R^2 = 0.37$). A similar loss of dependence was also reported by Guedes et al. (2011) in a field experiment on an intermediate beach.

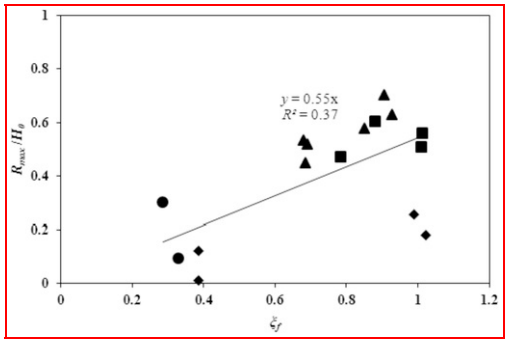

Fig. 16 Normalized maximum runup as a function of ξ_f - diamond symbols: spilling breaking on subtidal bar; circle symbols: spilling breaking with two breaking points; triangle symbols: spilling breaking at the shore; square symbols: plunging breaking at the shore.

alt-text: Fig. 16

Conditions of breaking (type: spilling, plunging and position: on the subtidal bar, near the shore) are spotted by different symbols in Fig. 17a. Present data emphasize that the maximum runup differs according to breaking conditions. When breaking occurs far from the shore, the increase of R_{max}/H_0 for increasing values of ξ_f is weaker than the one observed when breaking is localized near the shore. For example, when $\xi_f = 0.95$, a ratio of 3 is measured between the two runup estimations: with breaking near the shore and on the bar far from the shore (Fig. 17a). The linear increase of normalized runup with ξ_f when breaking occurs on the subtidal bar cannot be attributed to a weaker influence of ξ_f for low beach gradient as observed for dissipative beaches (Nielsen and Hanslow, 1991; Ruggiero et al., 2001; Stockdon et al., 2006). Measured foreshore slopes for low tide levels are not in the range of dissipative beaches.

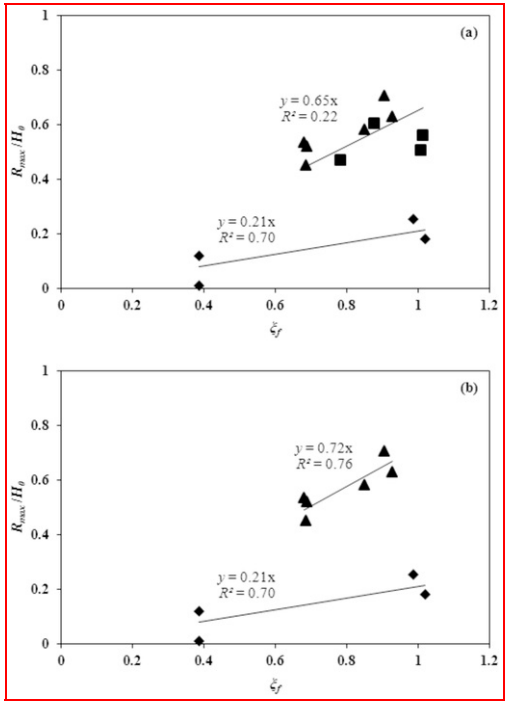

Fig. 17 Normalized maximum runup as a function of ξ_f for (a) different breaking conditions (b) spilling breaking. Breaking positions and type of breaking are differentiated for linear regression estimations-diamond symbols: spilling breaking on subtidal bar; triangle symbols: spilling breaking at the shore; square symbols: plunging breaking at the shore.

alt-text: Fig. 17

The breaking type also seems to influence the wave runup. Thus, for a same short length of surf zone, a plunging breaking produces a greater wave energy dissipation than a spilling breaking, resulting in lower runup values. This result is consistent with laboratory studies performed by Wang et al. (2002a) and Wang and Kraus (2005) which compare the rate of wave decay following the two types of breaking and conclude on a much greater dissipation rate for plunging breakings. Let us consider in Fig. 17b present results taking into account only the cases for which a spilling breaking occurs near the shoreline. The regression coefficient is significantly improved in this case: R^2 jumps from 0.22 to 0.76 (Fig. 17b). We did not analyze the case of a plunging breaking because of the limited number of measured values in this case. Present data show that the runup linearly depends on ξ_f but that this dependence differs according to breaking location.

Fig. 18 shows the influence of the surf slope on the normalized runup through the Irribaren number based on the deep wave height and the surf slope ξ_s. The breaking position is directly taken into account with the parameter ξ_s. Fig. 18 shows that the maximum runup fits well with the surf slope ($R^2 = 0.88$) with a higher regression coefficient than with the foreshore slope. Furthermore, the breaking type plays a negligible role. The Iribarren number based on the surf slope appears to be more representative of the whole data set. In the field study of Guedes et al. (2011) for a microtidal beach with tidal ranges between 1.2 and 2 m, it was shown that an estimation of the runup based on the foreshore slope does not give satisfactory results. These authors have outlined the shift of the break point from the sand bar towards the shoreline with the level of the tide. Such a shift has also been mentioned by Stockdon et al. (2006) in the case of microtidal and mesotidal beaches. Then, the use of the surf zone slope which takes into account the breaking position seems more adapted than the use of the foreshore slope for the parameterization of the extreme runup as well in the microtidal regime as in the macrotidal regime.

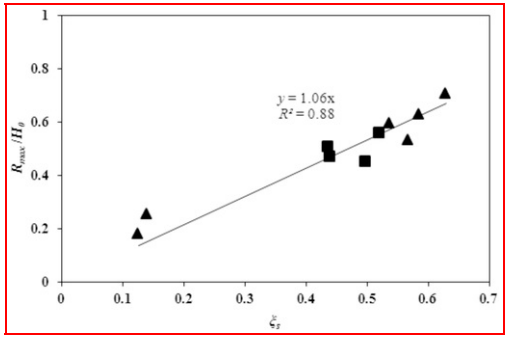

Fig. 18 Normalized maximum runup as a function of ξ_s - triangle symbols: spilling breaking; square symbols: plunging breaking.

alt-text: Fig. 18

Fig. 19 shows the maximum runup normalized by the breaking wave height plotted as a function of ξ_{sb}, Iribarren number based on the breaking wave height and the surf slope. It appears that, taking into account breaking wave height increases the correlation with present data ($R^2 = 0.93$). The use of the breaking height instead of the incident wave height seems to be more adapted for the parameterization of the extreme runup, as suggested by Enjalbert et al. (2012). Finally, the runup for the intermediate beaches - beach regime considered in the present study - can be estimated with the following equation:

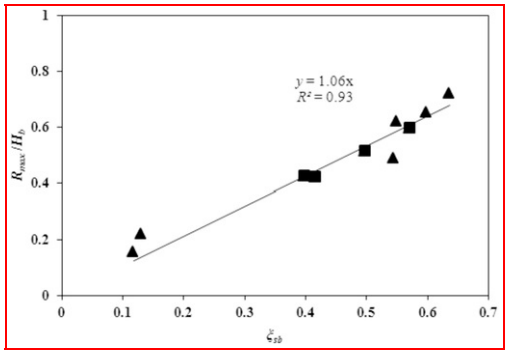

Fig. 19 Normalized maximum runup as a function of ξ_{sb} - triangle symbols: spilling breaking; square symbols: plunging breaking.

alt-text: Fig. 19

4.3 Maximum runup comparison with existing predictors

In this section, the ability of available extreme runup parameterizations to predict maximum runup for the present study is considered. We focus on the formulae corresponding to reflective and intermediate beaches (Table 1).

Three estimators are calculated to compare the performance of predictors (Table 6): the root-mean-square error (*RMSE*), the Pearson correlation coefficient (r) and the Mean Error (*ME*). The parameterizations are tested with the beach gradient chosen by the authors.

Table 6 Root-mean-square error (*RMSE*), Pearson correlation coefficient (r) and Mean Error (*ME*) between observed and calculated runup values.

alt-text: Table 6

Slope	Study	Equation	RMSE (cm)	r	*ME*
β_a	Cariolet (Cariolet, 2011)	Eq. (12)	0.65	0.93	−0.009
	Cariolet and Suanez (Cariolet and Suanez, 2013)	Eq. (13)	1.33	0.93	−0.013

β_f	Mase (Mase, 1989)	Eq. (18)	5.96	0.90	0.057
	Nielsen and Hanslow (Nielsen and Hanslow, 1991)	Eq. (7)	2.79	0.87	0.027
	Van der Meer and Starm (van der Meer and Stam, 1992)	Eq. (8)	1.74	0.86	0.015
	Ruggiero et al. (Ruggiero et al., 2001)	Eq. (22)	0.94	0.90	0.005
	Hedges and Mase (Hedges and Mase, 2004)	Eq. (15)	5.73	0.89	0.055
	Stockdon et al. (Stockdon et al., 2006)	Eq. (11)	0.95	0.87	0.003
		Eq. (23)	0.82	0.88	−0.002
	Cariolet and Suanez (Cariolet and Suanez, 2013)	Eq. (13)	0.82	0.86	0.003
	Blenkinsopp et al. (Blenkinsopp et al., 2016)	Eq. (16)	2.85	0.89	0.026
		Eq. (20)	3.01	0.92	0.029
	Park and Cox (Park and Cox, 2016)	Eq. (21)	3.70	0.91	0.038
β_s	Holman (Holman, 1986)	Eq. (14)	0.51	0.98	0.005
	Komar (Komar, 1998)	Eq. (10)	0.27	0.98	0
	Present equation	Eq. (31)	0.25	0.98	0

Table 6 shows that the formulae of Mase (1989) and Hedges and Mase (2004), based on impermeable laboratory beaches and using the foreshore slope are not adapted to the present study. They provide high wave runup values with high values of *ME* (Table 6). The runup values calculated using the formula of Park and Cox (2016) overestimate reality, with a root-mean-square error (RMSE) of 3.70 cm. For the formula suggested by Cariolet and Suanez (2013) (Eq. (13)), these authors indicate that the active slope of the beach coincides with the foreshore slope. We therefore consider the two slopes in our comparison. When using the slope of the active section of the beach, the formula provides low wave runup values ($RMSE = 1.33$ cm; $ME = -0.013$), whereas, the data fit is far better with the foreshore slope ($RMSE = 0.82$ cm; $ME = 0.003$). It suggests that this model cannot be applied in the present case using the active slope, case for which there is no coincidence between the two slopes.

Fig. 20 illustrates the comparison between measured and calculated values of runup for a selection of expressions performing the best results. Perfect agreement is shown by the solid line. Most of the parameterizations tends to overestimate the maximum runup when breaking is triggered by the sandbar (R_{max}<0.014 m), and to underestimate it when breaking occurs near the shore (R_{max}>0.023 m).

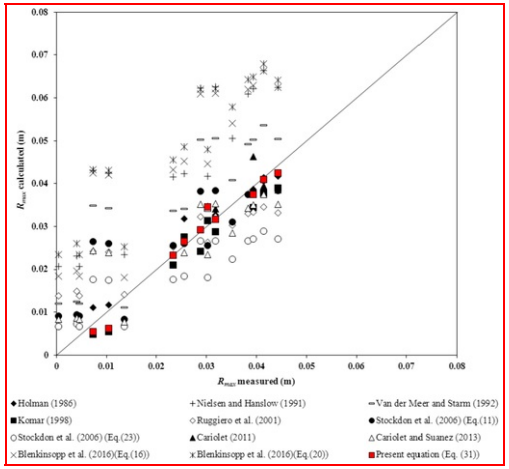

Fig. 20 Comparison between measured and calculated values for the maximum runup.

alt-text: Fig. 20

When the measured values are plotted against formulations based on the foreshore slope, results are closer to the observed values when breaking occurs near the shore (

Table 7). The wave breaking conditions are generally not specified in previous studies. However, as breaking occurs near the shore for reflective beaches, the formulae are more adapted to estimate maximum runup when breaking takes place near the shore.

Table 7 Root-mean-square error (*RMSE*) between predicted and observed values of runup according to the breaking position. (No indentation for 'study column' of Table 7 please. It has to be justified at left.)

alt-text: Table 7

Study	Equation	*RMSE* (cm) (all data)	*RMSE* (cm) (breaking on subtidal bar)	*RMSE* (cm) (breaking at the shore)
Nielsen and Hanslow (Nielsen and Hanslow, 1991)	Eq. (7)	2.79	3.20	2.77
Van der Meer and Starm (van der Meer and Stam, 1992)	Eq. (8)	1.74	2.30	1.62
Ruggiero et al. (Ruggiero et al., 2001)	Eq. (22)	0.94	1.63	0.44
Stockdon et al. (Stockdon et al., 2006)	Eq. (11)	0.95	1.60	0.59
	Eq. (23)	0.82	0.93	0.82
Cariolet and Suanez (Cariolet and Suanez, 2013)	Eq. (13)	0.82	1.42	0.47
Blenkinsopp et al. (Blenkinsopp et al., 2016)	Eq. (16)	2.85	3.04	2.84
	Eq. (20)	3.01	3.26	3.07

From Fig. 20 and Table 6, it can be noted that the formulations of Holman (1986) and Komar (1998) based on the surf slope provide the best estimation for the runup with a root-mean-square error (*RMSE*) of 0.51 cm and 0.27 cm, respectively. This conclusion is in agreement with our parametric study (Section 4.2). The formula proposed by Cariolet (2011), based on the active slope of the beach also gives a good agreement with present data ($RMSE = 0.65$ cm). The present formulation (Eq. (31)) based on the surf slope and the wave breaking height allows to further improve the agreement with runup acquired on the studied beaches.

5 Conclusion

The runup was investigated for intermediate beaches from a physical modelling in a wave flume under regular waves and tide. Wave breaking is modulated by the tide. It is triggered by the subtidal bar for lower tide levels and occurs near the shore for higher tide levels. For intermediate levels, two breaking locations are detected: one above the subtidal bar before wave reformation, and one near the shore. Komar and Gaughan (1972) formulation for the breaking height gives the best fit with present data for different breaking conditions.

The water surface elevation at the shore is decomposed in wave runup, swash height and wave setup for the three phases: rising, falling and high tide of the tidal cycle. Present results show the complexity of runup which depends on breaking conditions, beach morphology and phase of the tide. The rising and falling tides are decomposed into three zones according to the breaking zone. For a breaking above a subtidal bar and a mild beach slope, the wave runup and the swash height regularly increase with the water level. For intermediate tide levels, when two breaking points are observed, the runup decreases as the water level increases in spite of a steeper foreshore slope ($\beta_f = 0.160$). This is attributed to an increase of wave dissipation. For levels between the zero water level and the high tide level characterized by a breaking near the shore, important differences between rising and falling tides are exhibited. The shoreline elevation is more regular during the falling tide than during the rising tide. This is a consequence of the high sensitivity to the local beach morphology which is more complex in the rising phase, and by the smoothing of beach profile during the falling phase. Energetic waves reach the upper part of the beach during the high tide phase, and induce hydrodynamic and morphological changes leading to a runup decrease. The simultaneous monitoring of local beach slope and breaking conditions gives information on the hydrodynamic changes occurring in the swash zone. During the high tide phase, the upper beach erodes, the beach slope flattens and the breaking point slightly moves offshore with a change of breaking type from plunging to spilling. Swash events are more regular at the end of this phase when the beach profile has reached a stable morphology.

A detailed analysis of runup was performed. The parametric study highlights the major influence of the tidal level which directly affects parameters such as the incident wave energy, the breaking conditions (position, height and type) and the beach slope. The dependence of runup with the foreshore slope and the surf zone slope through the Iribarren number was also analyzed. The foreshore slope is less well correlated to the entire present dataset than

the surf slope. However, it can be used to predict the maximum runup when breaking occurs near the shore. Existing formulae based on the foreshore slope for the runup estimation are also globally less successful than those based on the surf slope since wave breaking conditions are not taken into account using the foreshore slope. The parametric study also shows that the use of the wave breaking height instead of the incident wave height is recommended for a correct estimation of maximum runup for intermediate beaches subjected to a strong tidal forcing. A new wave run up formula, based on the surf slope and the wave breaking height is proposed. It is clear that for field studies it is difficult to measure accurately the breaking position, especially when the bathymetry is complex. An alternative choice is to consider the active slope of the beach for the runup estimation for beaches in the intermediate regime, slope which is easy to measure in the field. Future field studies are necessary to confirm present experimental results.

Acknowledgements

This work was supported by the Normandy region (Scale Research Network).

References

Battjes J.A., Surf similarity, In: *Proceedings of the 14th Conference on Coastal Engineering (ASCE), Copenhagen, Denmark,* 1974, 466–480.

Blenkinsopp C., Matias A., Howe D., Castelle B., Marieu V. and Turner I., Wave runup and overwash on a prototype-scale sand barrier, *Coast. Eng.* **113**, 2016, 88–103.

Cariolet J.M., Quantification du runup sur une plage macrotidale à partir des conditions morphologiques et hydrodynamiques, *Géomorphol. Relief, Process. Environ.* **1**, 2011, 95–108.

Cariolet J.M. and Suanez S., Runup estimations on a macrotidal sandy beach, *Coast. Eng.* **74**, 2013, 11–18.

Dean R.G., Heuristic models of sand transport in the surf zone, In: *Proceedings of the First Australian Conference on Coastal Engineering, Sydney, Australia,* 1973, 208–214.

Enjalbert C., Sénéchal N., Bryan K.R., Coco G., MacMahan J. and Brown J., Dynamique de la zone de swash: influence de la marée et de la morphologie sur les paramètres du run-up, In: *Proceedings of XIIèmes Journées Nationales Génie Côtier – Génie Civil,* 2012, 51–58.

Goda Y., A synthesis of breaker indices, *Trans. JSCE* **2**, 1970, 227–230.

Goda Y., In: *Random Seas and Design of Marine Structures. Advanced Series on Ocean Engineering* **vol. 15**, 2000, World Scientific.

Grasso F., Michallet H., Barthélemy E. and Certain R., Physical modeling of intermediate cross-shore beach morphology: transients and equilibrium states, *J. Geophys. Res.* **114** (C9), 2009.

Guedes R.M.C., Bryan K.R., Coco G. and Holman R.A., The effects of tides on swash statistics on an intermediate beach, *J. Geophys. Res.* **116**, 2011, C04008.

Guza R.T. and Thornton E.B., Wave set-up on a natural beach, *J. Geophys. Res.* **86** (C5), 1981, 4133–4137.

Guza R.T. and Thornton E.B., Swash oscillations on a natural beach, *J. Geophys. Res.* **87** (C1), 1982, 483–491.

Hanslow D.J. and Nielsen P., Shoreline set-up on natural beaches, *J. Coast. Res. SI* **15**, 1993, 1–10.

Hedges T.S. and Mase H., Modified Hunt's equation incorporating wave setup, *J. Waterw. Port, Coast. Ocean Eng.* **130**, 2004, 109–113.

Holman R.A., Extreme value statistics for wave run-up on a natural beach, *Coast. Eng.* **9**, 1986, 527–544.

Holman R.A. and Sallenger A.H., Jr., Setup and swash on a natural beach, *J. Geophys. Res.* **90** (C1), 1985, 945–953.

Hunt I.A., Design of seawalls and breakwaters, *J. Waterw. Harb. Div.* **85**, 1959, 123–152.

Iribarren C.R. and Nogales C., Protection des ports, In: *XVIIth International Navigation Congres,* **1**, 1949.

Khoury A., Jarno-Druaux A. and Marin F., Experimental simulation of sandy beaches under waves and tides: hydro-morphodynamic analysis, *J. Coast. Res. SI* **65**, 2013, 1791–1796.

Komar P.D., Beach Processes and Sedimentation, second ed., 1998, Prentice-Hall; Upper Saddle River, New Jersey.

Komar P.D. and Gaughan M.K., Airy wave theory and breaker height prediction, In: *Proceedings of the 13th Coastal Engineering Conference* 1972, ASCE); Vancouver, 405–418.

Levoy F., Anthony E.J., Monfort O. and Larsonneur C., The Morphodynamics of megatidal beaches in Normandy, France, *Mar. Geol.* **171**, 2000, 39–59.

Mase H., Random wave runup height on gentle slope, *J. Waterw. Port, Coast. Ocean Eng.* **115**, 1989, 649–661.

Mase H. and Iwagaki Y., Run-up of random waves on gentle slopes, *Coast. Eng.* **1** (19), 1984, 2156, 1028.

Masselink G. and Hughes M.G., Field investigation of sediment transport in the swash zone, *Cont. Shelf Res.* **18** (10), 1998, 1179–1199.

Nielsen P., Wave setup: a field study, *J. Geophys. Res.* **93** (C12), 1988, 15643–15652.

Nielsen P., *Coastal and Estuarine Processes. Advanced Series on Ocean Engineering* **vol. 29**, 2009, World Scientific.

Nielsen P. and Hanslow D.J., Wave runup distributions on natural beaches, *J. Coast Res.* **7**, 1991, 1139–1152.

Park H. and Cox D.T., Empirical wave run-up formula for wave, storm surge and berm width, *Coast. Eng.* **115**, 2016, 67–78.

Puleo J.A., Beach R.A., Holman R.A. and Allen J.S., Swash zone sediment suspension and transport and the importance of bore-generated turbulence, *J. Geophys. Res.* **105**, 2000, 17021–17044.

Ruessink B.G., Kleinhaus M.G. and van den Beukel P.G.L., Observations of swash under highly dissipative conditions, *J. Geophys. Res.* **103** (C2), 1998, 3111–3118.

Ruggiero P., Komar P.D., McDougal W.G., Marra J.J. and Beach R.A., Wave runup, extreme water levels and the erosion of properties backing beaches, *J. Coast Res.* **17** (2), 2001, 407–419.

Sabatier F., Anthony E.J., Héquette A., Suanez S., Musereau J., Ruz M.H. and Regnault H., Morphodynamics of beach/dune systems: examples from the coast of France, *Géomorphol. Relief, Process. Environ.* **1**, 2009, 3–22.

Saleh Salem A., Modélisation physique en canal à houle de la morphodynamique des plages sableuses, Ph.D. thesis2011, University of Le Havre; France.

Saleh Salem A., Jarno-Druaux A. and Marin F., Physical modeling of cross-shore beach morphodynamics under waves and tides, *J. Coast. Res. SI* **64**, 2011, 139–143.

Sánchez-Arcilla A., Cáceres I., van Rijn L. and Grüne J., Revisiting mobile bed tests for beach profile dynamics, *Coast. Eng.* **58**, 2011, 583–593.

Senechal N., Coco G., Bryan K.R. and Holman R.A., Wave runup during extreme storm conditions, *J. Geophys. Res. Ocean.* **116** (C7), 2011, C07032.

Soulsby R., Dynamics of Marine Sands, 1997, Thomas Telford Publications; London, UK.

Stockdon H.F., Holman R.A., Howd P.A. and Sallenger A.H., Empirical parameterization of setup, swash, and runup, *Coast. Eng.* **53** (7), 2006, 573–588.

van der Meer J.W. and Stam C.M., Wave runup on smooth and rock slopes of coastal structures, *J. Waterw. Port, Coast. Ocean Eng.* **118**, 1992, 534–550.

Wang P. and Kraus N.C., Beach profile equilibrium and patterns of wave decay and energy dissipation across the surf zone elucidated in a large-scale laboratory experiment, *J. Coast Res.* **21** (3), 2005, 522–534.

Wang P., Smith E.R. and Ebersole B.A., Large-scale laboratory measurements of longshore sediment transport under spilling and plunging breakers, *J. Coast Res.* **18**, 2002, 118–135.

Wright L.D. and Short A.D., Morphodynamic variability of surf zones and beaches: a synthesis, *Mar. Geol.* **56**, 1984, 93–118.

Highlights

- Laboratory study of intermediate beaches in a wave flume with tide simulation.
- Processes governing beach profile changes during a tidal cycle.
- Parametric study of runup: breaking conditions and beach slopes are tested.

- New formula of runup based on surf slope and wave breaking height.
- Comparison between present experimental results and runup prediction formulae.

Queries and Answers

Query: Please confirm that the provided emails “alaa.khoury@univ-lehavre.fr, francois.marin@univ-lehavre.fr, jarnoa@univ-lehavre.fr” are the correct address for official communication, else provide an alternate e-mail address to replace the existing one, because private e-mail addresses should not be used in articles as the address for communication.
Answer: "alaa.khoury@univ-lehavre.fr' must be replaced by 'alaa.khoury@doct.univ-lehavre.fr'. We confirm the two other e-mail addresses.

Query: Have we correctly interpreted the following funding source(s) you cited in your article: Normandy region (Scale Research Network); etc.?
Answer: Yes

Query: Please confirm that given names and surnames have been identified correctly and are presented in the desired order and please carefully verify the spelling of all authors’ names.
Answer: Yes

Query: Your article is registered as a regular item and is being processed for inclusion in a regular issue of the journal. If this is NOT correct and your article belongs to a Special Issue/Collection please contact s.natarajan.2@elsevier.com immediately prior to returning your corrections.
Answer: Yes

Query: The supplied pixels-based source image has a very low image resolution (not enough pixels for the print size) and hence is not directly usable. Please provide us with an image that has a minimum resolution of 300 dots per inch (dpi) and a proper print size. For example, a single column can be around 85 mm wide, and then the raster image needs to be around 900 pixels wide to meet this criterion. It is worthwhile to note that simply upsampling the image to create the right number of pixels will only make the image worse. A better action, most likely, is to export the original image from the software program in which it was put together as an EPS or PDF vector image, or else to export to TIFF by specifying the output print size and resolution in that application, according to these guidelines. You may refer to www.elsevier.com/locate/authorartwork for more details
Answer: We have improved the quality of the figure.

Query: The supplied pixels-based source image has a very low image resolution (not enough pixels for the print size) and hence is not directly usable. Please provide us with an image that has a minimum resolution of 300 dots per inch (dpi) and a proper print size. For example, a single column can be around 85 mm wide, and then the raster image needs to be around 900 pixels wide to meet this criterion. It is worthwhile to note that simply upsampling the image to create the right number of pixels will only make the image worse. A better action, most likely, is to export the original image from the software program in which it was put together as an EPS or PDF vector image, or else to export to TIFF by specifying the output print size and resolution in that application, according to these guidelines. You may refer to www.elsevier.com/locate/authorartwork for more details
Answer: We have improved the quality of the figure.

Query: The supplied pixels-based source image has a very low image resolution (not enough pixels for the print size) and hence is not directly usable. Please provide us with an image that has a minimum resolution of 300 dots per inch (dpi) and a proper print size. For example, a single column can be around 85 mm wide, and then the raster image needs to be around 900 pixels wide to meet this criterion. It is worthwhile to note that simply upsampling the image to create the right number of pixels will only make the image worse. A better action, most likely, is to export the original image from the software program in which it was put together as an EPS or PDF vector image, or else to export to TIFF by specifying the output print size and resolution in that application, according to these guidelines. You may refer to www.elsevier.com/locate/authorartwork for more details
Answer: We have improved the quality of the figure.

Query: The supplied pixels-based source image has a very low image resolution (not enough pixels for the print size) and hence is not directly usable. Please provide us with an image that has a

minimum resolution of 300 dots per inch (dpi) and a proper print size. For example, a single column can be around 85 mm wide, and then the raster image needs to be around 900 pixels wide to meet this criterion. It is worthwhile to note that simply upsampling the image to create the right number of pixels will only make the image worse. A better action, most likely, is to export the original image from the software program in which it was put together as an EPS or PDF vector image, or else to export to TIFF by specifying the output print size and resolution in that application, according to these guidelines. You may refer to www.elsevier.com/locate/authorartwork for more details
Answer: We have improved the quality of the figure.

Query: The supplied pixels-based source image has a very low image resolution (not enough pixels for the print size) and hence is not directly usable. Please provide us with an image that has a minimum resolution of 300 dots per inch (dpi) and a proper print size. For example, a single column can be around 85 mm wide, and then the raster image needs to be around 900 pixels wide to meet this criterion. It is worthwhile to note that simply upsampling the image to create the right number of pixels will only make the image worse. A better action, most likely, is to export the original image from the software program in which it was put together as an EPS or PDF vector image, or else to export to TIFF by specifying the output print size and resolution in that application, according to these guidelines. You may refer to www.elsevier.com/locate/authorartwork for more details
Answer: We have improved the quality of the figure.

Query: The supplied pixels-based source image has a very low image resolution (not enough pixels for the print size) and hence is not directly usable. Please provide us with an image that has a minimum resolution of 300 dots per inch (dpi) and a proper print size. For example, a single column can be around 85 mm wide, and then the raster image needs to be around 900 pixels wide to meet this criterion. It is worthwhile to note that simply upsampling the image to create the right number of pixels will only make the image worse. A better action, most likely, is to export the original image from the software program in which it was put together as an EPS or PDF vector image, or else to export to TIFF by specifying the output print size and resolution in that application, according to these guidelines. You may refer to www.elsevier.com/locate/authorartwork for more details
Answer: We have improved the quality of the figure.